Experimental and numerical modeling of DC corona discharge in Wire-Cylinder-Plane configuration

Ahmed Kasdi, Sabrina Chouali, Adel Bekakria, Lucian Dascalescu

Experimental and numerical modeling of DC corona discharge in Wire-Cylinder-Plane configuration

Ahmed KASDI [a*], Sabrina CHOUALI [a], Adel BEKAKRIA[a], Lucian DASCALESCU [b]

[a] Laboratoire de Génie Electrique, Université de Bejaia, 06000, Algeria.

[b] Institut PPRIME, CNRS - Université de Poitiers – ENSMA, IUT, Angoulême, 16000, France.

[*]**ahmed.kasdi@univ-bejaia.dz**

Abstract

The aim of this paper is to present a numerical and experimental study of the positive corona discharge in the Wire-Cylinder-Plane geometry intended for electrostatic charging of insulating materials. A detailed experimental procedure is described to determine the corona discharge characteristics where different electrode layouts have been tested to improve the performance of the charge process. In addition, the corona governing equations are successfully implemented and solved in the studied geometry using Comsol Multiphysics Software. The study focused on the effect of the presence of the non-ionizing cylinder on the coronating wire. It has been found that increasing the diameter of the cylinder or bringing it closer to the wire reinforces the shielding effect between the two electrodes, which results in the reduction of the corona current and current density at the level of the measurement plane. The measured *I-V* characteristics and current density distributions were found to be in good agreement with the corresponding numerical predictions.

Keywords: Corona discharge, space charge, current density, ionized fields, electrostatic charge, shielding effect.

1. Introduction

Theoretical and experimental research has been executed for numerous a long time in order to understand and control the corona effect. Indeed, many of these studies were aimed at reducing its harmful effects which manifest themselves on high voltage electric power transmission lines [1-4]. Currently, the corona discharge is at the basis of several industrial applications, such as electrostatic dust precipitation [5], surface treatment [6-7], ozone generation [8-9], painting and spraying powders [10], granular mixtures separation [11-12], etc. In addition, corona discharge is exploited for charging dielectric materials for many practical applications in various configurations of electrodes [13-16].

The process of the electrical charging of the media is then obtained by using the corona effect often generated between an active energized electrode with a small radius of curvature and a passive earthed electrode with a larger radius of curvature [17-18]. Currently, a new type of electrodes, the Wire-Cylinder-Plane type, is increasingly used in various electrostatic applications [19-22]. In this configuration, the corona discharge is developed between a grounded collector plate and a dual electrode, consisting of a thin ionizing wire supported by a non-ionizing metal cylinder, the two electrodes being stressed with the same high voltage.

The purpose of the present work is to study the efficiency of the process of electrostatic charging which depends in particular on the various geometric parameters of the used electrode system. Indeed, the works carried out until now, and which deal with this geometry, have never explored the effect of the dimension of the non-ionizing cylinder or of its distance from the active wire. With this in mind, we have tested the influence of variations of the cylinder radius, the wire-to-cylinder spacing and the wire-to-plane distance.

2. Materials and methods

An overview of the experimental setup is shown in Fig. 1. The corona discharge is generated in a Wire-Cylinder-Plane (WCP) geometry which consist of an ionized electrode (1), a constantan wire with a diameter of 0.4 mm, attached to a non-ionized metallic cylinder (2) of 40 mm in diameter. The dual electrode (Wire-Cylinder), fixed by two insulating supports (3), is carried at a high voltage V_a, provided by the DC-HV source of 0 to ±140 kV, 0.08 A.

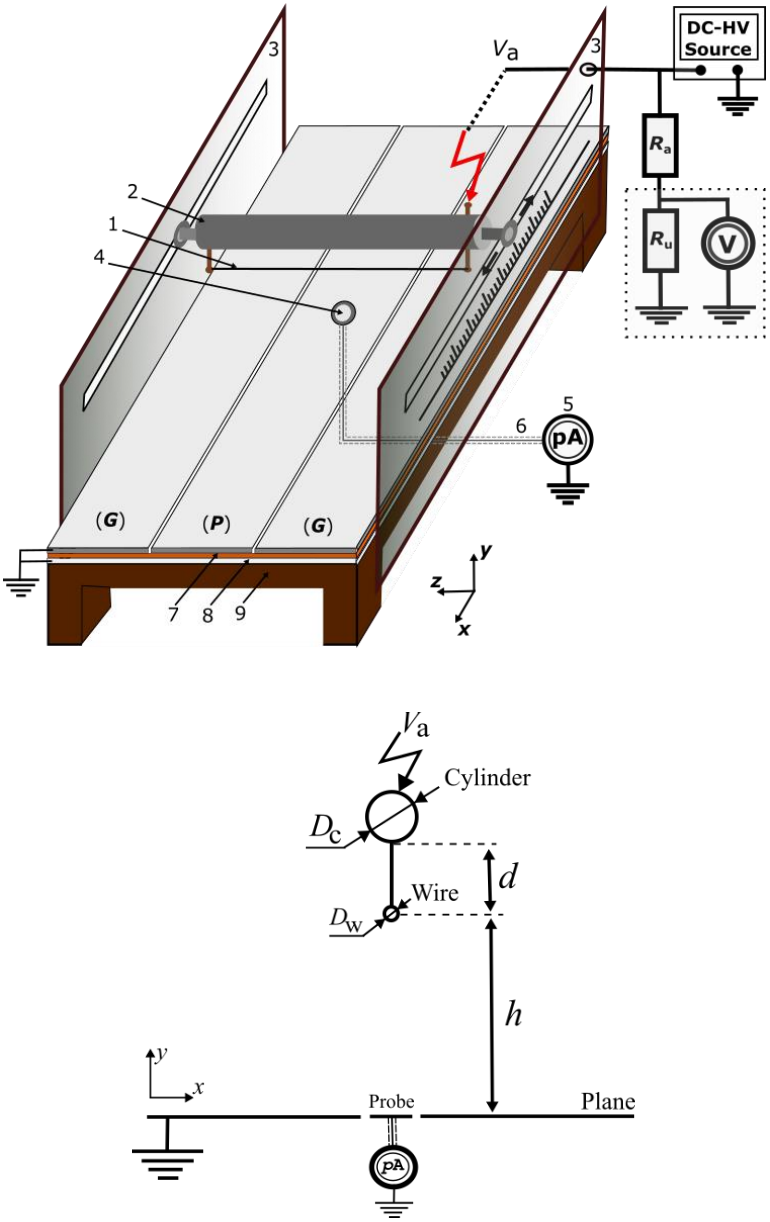

Fig.1. Schematic view of the experimental arrangement

A set of three plate electrodes, composed of a measuring plane (*P*) surrounded by two grounded guard plates (*G*), is placed at a distance *h* from the wire. Each plate is of dimensions 147 × 780 mm^2, 1 mm thickness, and is made of stainless steel. The three plates are separated by very small spacers to ensure the continuity of the electric field. A current collector (4), incorporated in the centre of the measurement plane (*P*), is connected to a current measuring device (5) by a coaxial cable (6). The plane electrodes rest on two plates; one is insulating (7) while the other is conductive (8) connected to the ground, all mounted on a wooden stand (9).

In order to be able to record the spatial distribution of the current density on the measurement plane, the insulating supports (3) are free to move in the horizontal x-direction, so that the current collector (4) moves relative to the Dual-electrode along the ground plane [5].

The experimental investigation made it possible to study the effect of variation of various geometrical parameters such as the cylinder diameter D_c (22, 26, 30 and 40mm), the wire-cylinder spacing *d* (20, 30 and 40 mm) and the wire-plane distance *h* (30, 40, 50 and 60 mm).

As the corona discharge largely depends on the atmospheric conditions [23], in particular the threshold of the appearance of the discharge, we proceeded during the tests to the measurement of the atmospheric pressure, the temperature and the relative humidity of the air.

3. Modeling and Numerical Procedure

Corona Discharge is a phenomenon that occurs in a gas in the vicinity of a highly stressed conductor of a small radius of curvature. Electric field close to the conductor is very important but remains not-disruptive. This provides condition for ionization of gas molecules in the nearest vicinity of corona electrode. As a result, two distinct regions are formed: a high-field thin region (ionization region) surrounding the active electrode and containing as many positive as negative charges (free-charge), and a drift region of low-field where charged particles move towards the passive collecting electrode [23-25]. The ionic space charges produced by corona affects significantly the electric field and cause its distortion, and in turn electric field affects the space charge distribution.

By considering the positive corona discharge as uniform along the length of the active wire, and with edge effects neglected, we can perform a two-dimensional (2D) analysis of the problem (Fig. 2). The DC corona electric field-space charge problem can then be described in the air by a set of the following equations [1,17,24]:

$$\Delta\phi = -\rho/\varepsilon_0 \text{ (The Poisson's equation)} \quad (1)$$

$$\vec{J} = \mu\rho\vec{E} \text{ (Equation for current density)} \quad (2)$$

$$\nabla.\vec{J} = 0 \text{ (Current continuity condition)} \quad (3)$$

$$\vec{E} = -\nabla\phi \text{ (Equation relating the potential to the field)} \quad (4)$$

Where ϕ [V] is the electric potential, *E* [V/m] is the electric field, *J* [A/m^2] is the current density, ρ [C/m^3] is the ionic charge density, ε_0 [F/m] is the air permittivity and μ [m^2/V.s] is the ionic mobility.

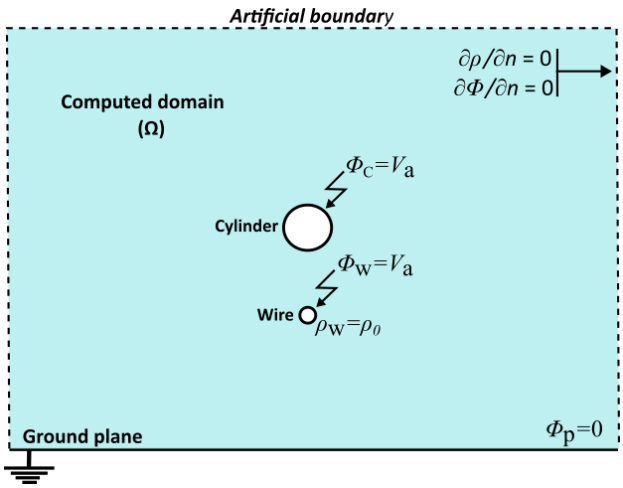

Fig. 2. 2D Geometry view of simulated WCP geometry with the defined boundary conditions

These corona governing equations clearly show the physical interactions between the electric field and the space charge density. After some straightforward manipulations of equations (1)-(4), we obtain:

$$\nabla^2\phi = -\rho/\varepsilon_0 \tag{5}$$

$$\vec{E}\nabla\rho = -\rho^2/\varepsilon_0 \tag{6}$$

The two above equations are coupled to each other, and it is difficult to solve them analytically because of the physical interaction between the electric field and the space charge density. For that, a numerical simulation is an alternate option.

In this work, the corona coupled equations (5)-(6) are solved numerically using the COMSOL Multiphysics software, which based on finite element method (*FEM*). Two application modes are adopted in a steady state regime; the *Electrostatic mode* (*es*), used to determine the electric potential distribution via Poisson's equation (5), and the *Charge Transport mode* (*ct*) used to resolve the current continuity equation (6) for finding the space charge density [5].

Furthermore, corona governing equations are subject to the following appropriate boundary conditions:

- The potential of the ionizing wire and non-ionizing cylinder is equal to the applied voltage: $\phi_w = \phi_c = V_a$,
- The potential of the plate is set to zero (ground): $\phi_p = 0$,
- Zero diffusive flux condition, $\partial\rho/\partial n = 0$, is imposed on all boundaries except at wire's surface where the charge density is fixed to an initial value ρ_0, which is adjusted iteratively until an auxiliary condition is satisfied [5]. Based on the Kaptzov's assumption [26], this auxiliary condition requires that the electric field strength at the surface of wire (E_w) remains constant at the threshold field value E_p, given by the Peek's empirical law [27]:

$$E_p = E_0\delta\eta\left(1 + \frac{0.308}{\sqrt{\delta R_w}}\right) \tag{7}$$

Where : E_0 =3.1×10^6 V/m is the dielectric breakdown strength of air, δ the relative air density factor with respect to SATP (25°C and 760 mmHg), η is the surface irregularity factor (η =1 for smooth surface) and R_w is the wire radius (in cm).

4. Results and Discussion

In this section, we present the results of experimental and numerical modeling of corona discharge generated in the Wire-Cylinder-Plane geometry. The numerical values of the geometric and physical parameters used for the simulation are given in Table 1.

Table 1: Parameters for the simulation

Symbol	Description	value
D_w	Wire diameter	0.4 mm
D_C	Cylinder diameter	22, 26, 30 and 40 mm
d	Wire-cylinder spacing	20, 30 and 40 mm
h	Wire-plane distance	30, 40, 50 and 60 mm
μ	Ion mobility	2×10^{-4} m^2/V.s
ε_0	Permittivity of the air	8.85×10^{-12} F/m
L_w	Length of the wire	147 mm
L_p	Length of the ground plane	780 mm
H_D	Height of the domain	400 mm
E_p	Threshold field	9.41×10^{6} V/m
δ_{E_w}	Pre-specified precision for the evaluation of the wire surface electric field according to Kaptzov's assumption.	1 %

4.1 Current voltage characteristics

During the corona discharge, a current depending on the applied voltage flows between the active and the passive electrode. The corona phenomenon can then be globally characterized by a current-voltage (I-V) relationships which follows the well known quadratic law of Townsend [28] :

$$I = KV(V - V_0) \tag{8}$$

Where I is the total corona current, V the applied voltage, V_0 the corona onset voltage and K a dimensional constant depending on the operating conditions.

Figs. 3-5 below illustrate the measured and calculated current-voltage characteristics of the corona discharge for different studied configurations. For low applied voltages, no current is detected. When the value of the applied voltage reaches the corona onset voltage V_0, the current starts flowing from the wire to the plane because of the ionization of air between electrodes. For high values of applied voltage, the current increases rapidly.

The corona discharge current is determined in the Comsol program by integrating the current density along the coronating wire. The predictions given by the numerical model agree well with the experimental curves.

4.1.1 Effect of wire-to-plane spacing h

We show in Fig. 3 the impact of changing the wire-to-plane spacing h on the I–V characteristics. It clearly appears that the discharge current is greater and increases more rapidly, with the applied voltage, for smaller inter-electrode distances. Obviously, this is due to the fact that, in any corona discharge configuration, increasing the distance between the active and passive electrodes yields to increasing the corona discharge threshold voltage [29,30], and consequently the decrease of the corona current.

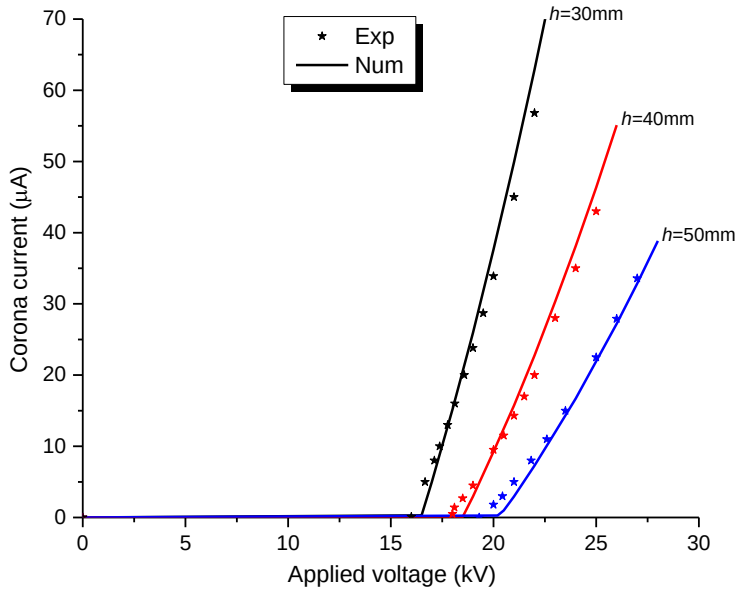

Fig. 3. Current-voltage characteristics for different wire-to-plane spacing h (D_w=0.4 mm, D_c=26 mm, d=30 mm).

4.1.2 Effect of wire-to-cylinder spacing d

Fig. 4 illustrates the current-voltage characteristics of studied geometry for two different values of the wire-to-cylinder spacing d, namely 20 and 30 mm. From the figure we can see that, for the same applied voltage, the decrease in the wire-cylinder spacing causes the diminution of the total corona discharge current. This is due to the shielding effect exerted by the cylinder on the ionizing wire, involving the reduction of the development of the corona discharge [5,31,32].

4.1.3 Effect of cylinder diameter Dc

We show in Fig. 5 the influence of varying the diameter D_c of the cylinder on the I–V curves. According to this figure, it can be seen that the smaller the diameter D_c, the higher the magnitude of the discharge current. This is explained by the fact that the diminution in the diameter of the cylinder leads to a reduction in the shielding effect on the coronating wire.

4.2 Current density distribution at the ground plane

The current density distribution on the ground plate is determined by connecting the measurement plane (P) to the earth and the current probe (4) to the picoammeter (5). The plane current density values are calculated as :

$$J = \frac{I_P}{S_P} \tag{9}$$

Where I_P is the probe's current and S_P the area of the probe.

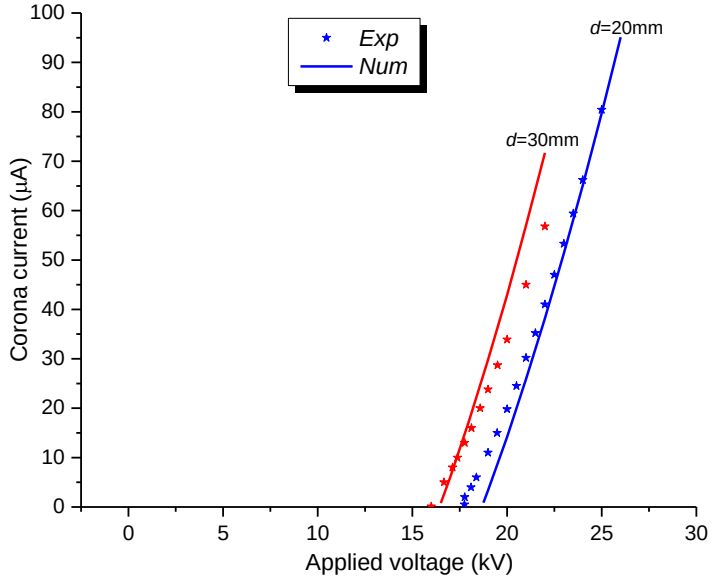

Fig. 4. Current-voltage characteristics for different wire-to-cylinder spacing d (D_w=0.4 mm, D_c=26 mm, h=30mm).

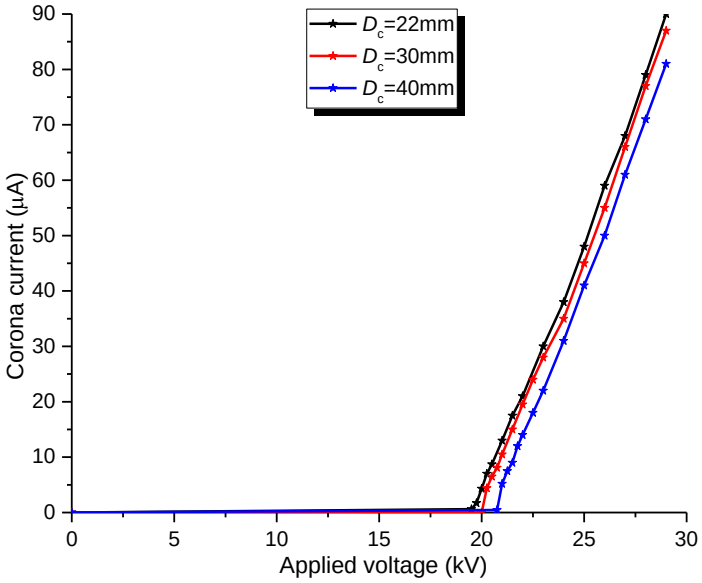

Fig. 5. Current-voltage characteristics for different cylinder diameter D_c (D_w=0.4 mm, d=20mm, H=40mm).

4.2.1 Effect of the applied voltage amplitude V_a

Fig. 6 shows the calculated and measured current density curves along the collecting plane of the WCP geometry under three applied voltage levels (20, 23 and 26 kV). The current density profile takes a bell-shape (analogous to the well-known Warburg's law [33]), with a peak value at the foot of the ionized wire and tends to zero further away. In addition, as we increase the magnitude of the applied voltage V_a, the current density will increase sensibly. On the other hand, as can be seen from the figure, the plane current density distributions predicted by the Comsol program agree well with the measured curves.

4.2.2 Effect of the inter-electrode spacing h

The influence of the inter-electrode spacing *h* on the distributions of the current density at the ground plane is shown at Fig. 7. By increasing the distance *h* between the wire and the plane, the current density values decreases considerably. As mentioned above, this is due to the diminution of the corona discharge current with the increasing of the height *h*, due to the rising of the onset corona voltage.

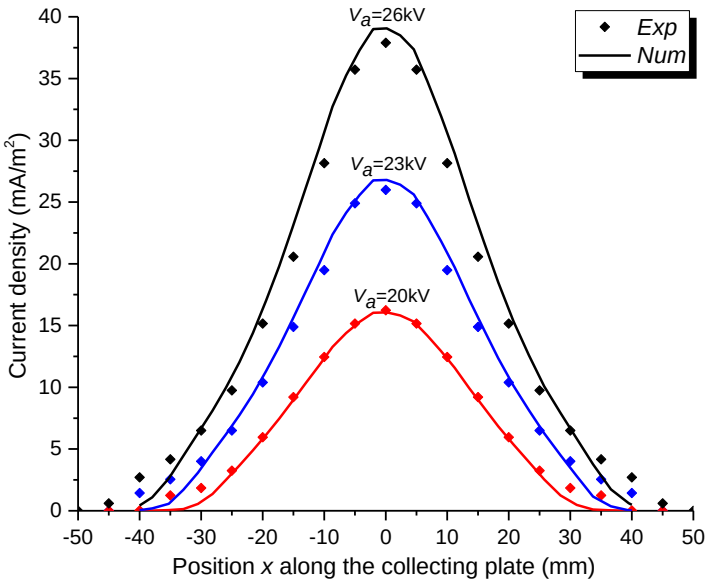

Fig. 6. Ground current density distributions of WCP geometry for different applied voltage amplitudes (D_w=0.4 mm, D_c=30mm, d=40mm, H=30mm).

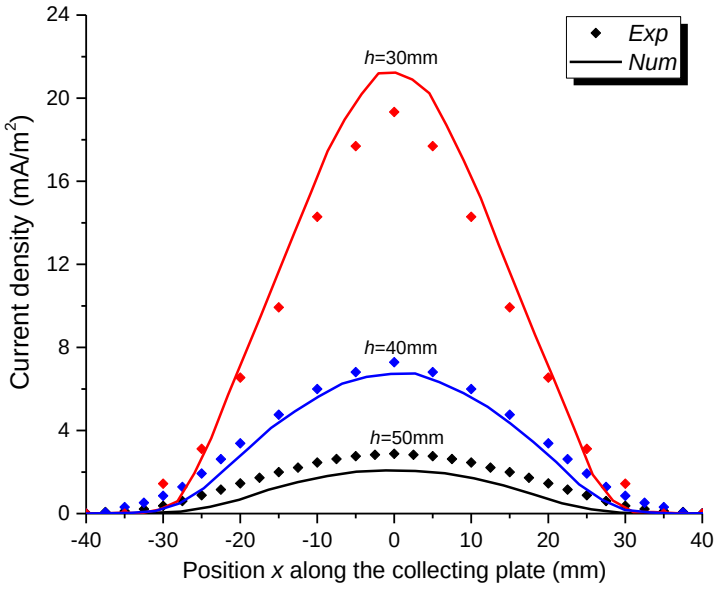

Fig. 7. Ground current density distributions of WCP geometry for different inter-electrode spacing *h* (D_w=0.4 mm, D_c=26mm, d=30 mm, V_a=22kV).

4.2.3 Effect of the wire-cylinder spacing d

Fig. 8 shows the calculated and measured ground current density distributions as a function of wire-cylinder spacing *d*. Reducing the distance *d* decreases the magnitude of the current density at the ground plane. Indeed, as mentioned above, bringing the cylinder closer to the wire increases the shielding effect and reduces the current.

Through the realized simulation program, we can plot the variation curves of the ground plane current density for several cylinder-wire distances *d*, Fig. 9. According to this figure, by increasing the interval *d*, the current density increases continuously and then saturates for values of d >70 mm. Indeed, the augmentation of the wire-cylinder spacing reduces the shielding effect between the two electrodes and from this threshold value the presence of the cylinder has no effect, the configuration is then similar to the wire-plane geometry (black dashed curve).

4.2.4 Effect of cylinder diameter Dc

Fig. 10 shows the impact of varying the cylinder diameter D_C on the ground current density distributions. The current density values decrease when the diameter D_C increases due to the shielding effect. This result is also confirmed by Fig. 11 which shows the calculated distributions of J for several values of the cylinder diameter D_C. As shown in this figure, by decreasing the diameter D_C, the current density increases continuously to approach the value of J calculated for a Wire-Plan configuration (dashed curve in black). Indeed, when the diameter of the cylinder is small, its effect on the ionizing wire is drastically reduced, the configuration is then similar to the wire-plane geometry.

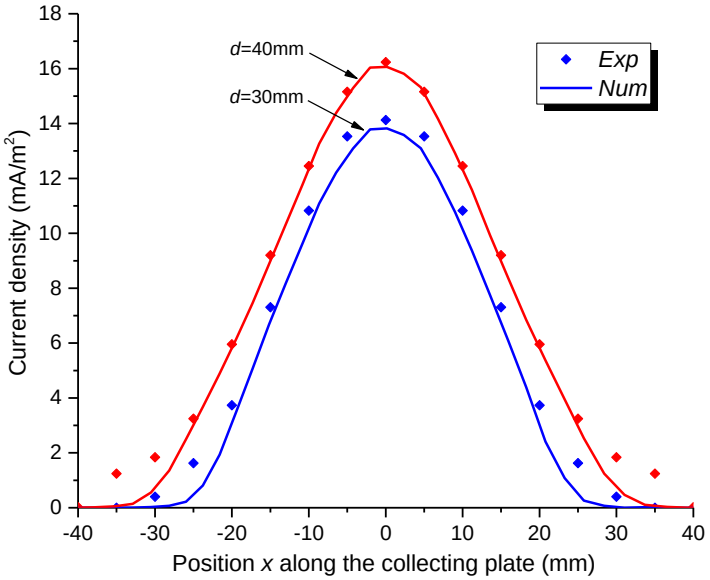

Fig. 8. Influence of the wire-cylinder spacing *d* on the ground current density distributions (D_w=0.4 mm, D_c=30mm, h=30mm, V_a=20kV).

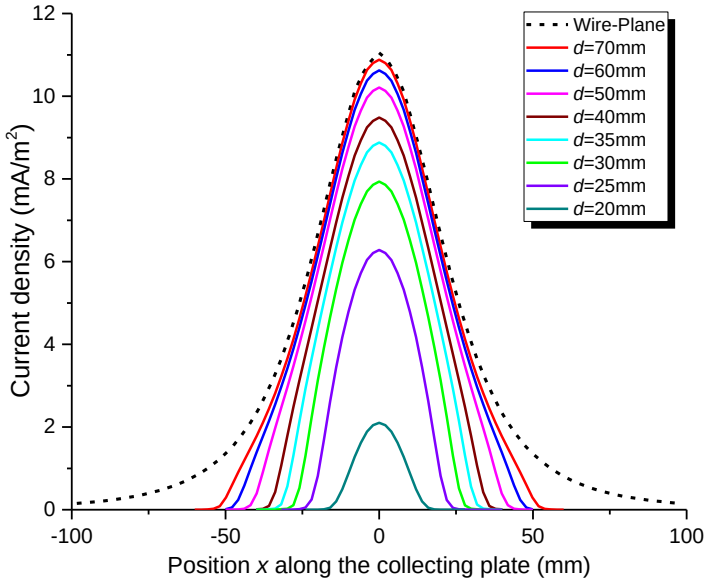

Fig. 9. Effect of wire-cylinder spacing d on the Calculated ground current density (D_w=0.4 mm, D_c=40mm, h=40mm, V_a=23kV).

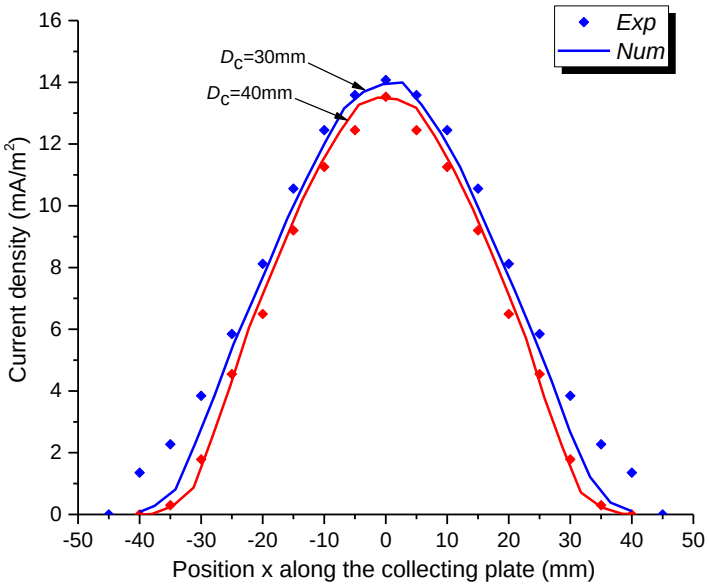

Fig. 10. Influence of cylinder diameter D_c on the ground current density distributions (D_w=0.4 mm, d=30mm, H=40mm, V_a=26kV).

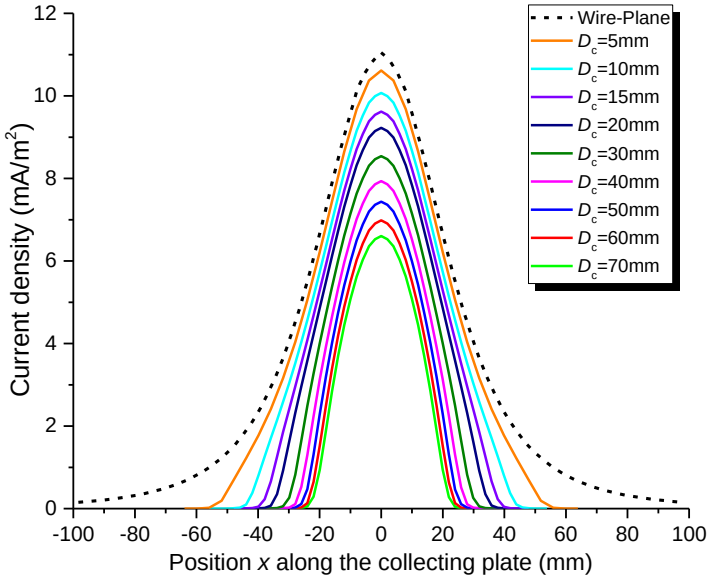

Fig. 11. Calculated ground current density distributions for different cylinder diameter D_c (D_w=0.4 mm, d=30mm, h=40mm, V_a=23kV).

4.3 2D distributions of the electric potential, electric field and space charge density

Other important corona discharge parameters that have not been measured such as electric potential, electric field or space charge density are obtained using Comsol Multiphysics. The modeling software makes it possible to plot the calculated variables in the inter-electrode space with a two-dimensional representation using graphical colors as shown in Figs. 12-14.

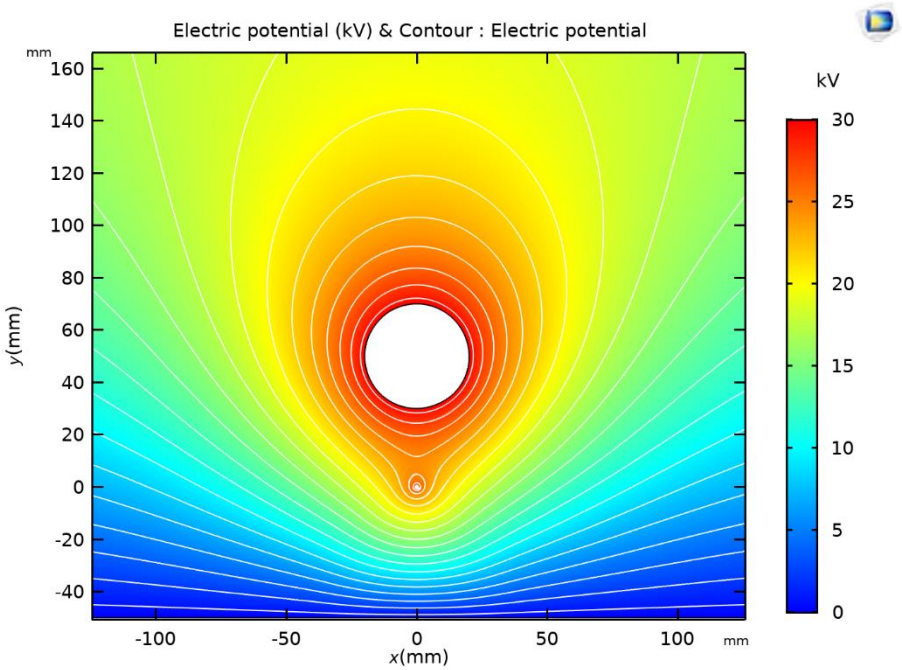

Fig. 12 : *Simulated spatial distribution of the electric potential in D-WCP geometry* (D_w=0.4 mm, D_c=40mm, d=30mm, h=50mm, V_a=30kV).

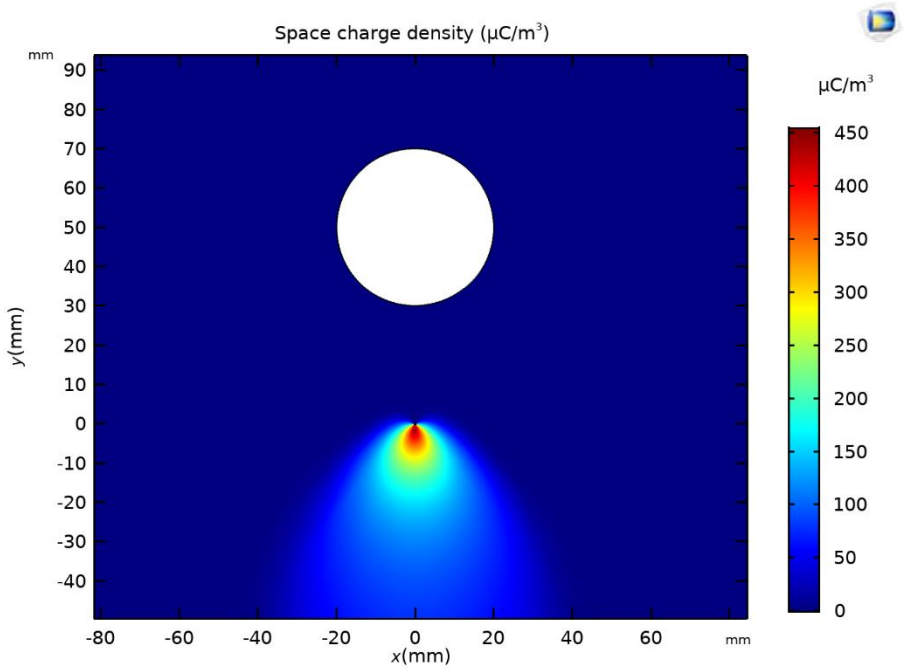

Fig. 13 : *Simulated spatial distribution of space charge density in D-WCP geometry* (D_w=0.4 mm, D_c=40mm, d=30mm, h=50mm, V_a=30kV).

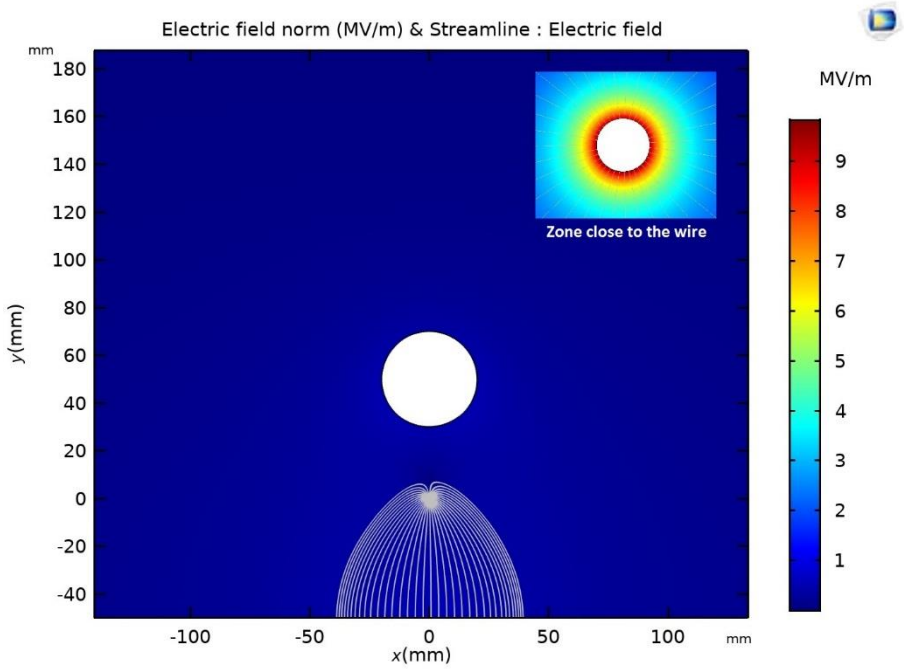

Fig. 14 : *Simulated spatial distribution of the electric field in D-WCP geometry* (D_w=0.4 mm, D_c=40mm, d=30mm, h=50mm, V_a=30kV).

In these figures, the effect of the presence of the non-ionizing cylinder on the coronating wire is clearly seen. Indeed, according to Figs. 13 and 14, the calculated space charge density is concentrated under the wire and the electric field lines are oriented towards the ground plane. This is obviously due to the shielding effect exerted by the cylinder on the wire.

To illustrate this, we present in Fig. 15 the simulated space charge density and electric field distributions in the Wire-Plane geometry. In the absence of the cylinder, the space charge is less concentrated under the wire and the field lines are more dispersed in the inter-electrode space.

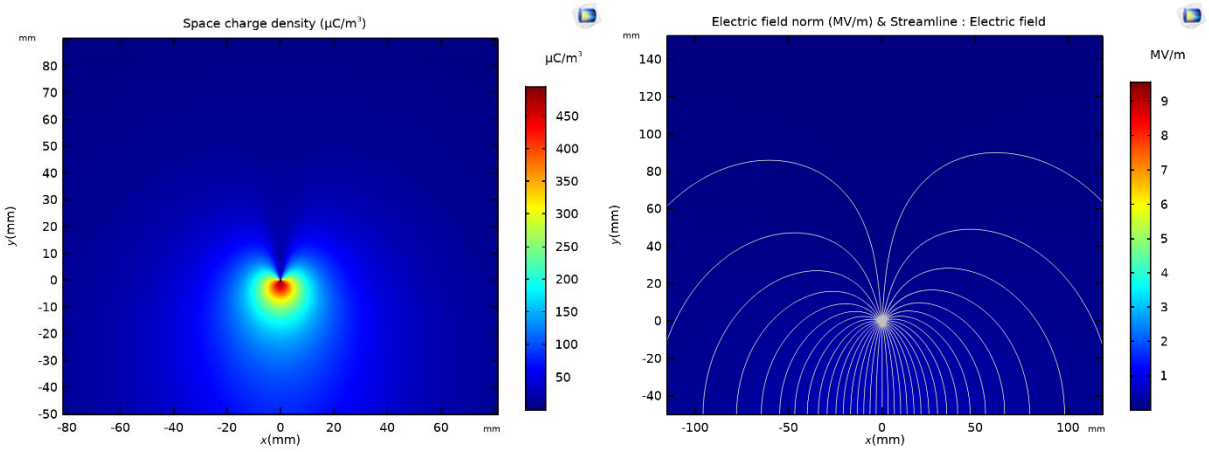

(a) (*b*)

Fig. 15 : *2D distributions of the space charge density (a) and the electric field (b) in Wire-Plane geometry* (D_w=0.4 mm, h=50mm, V_a=30kV).

5. Conclusion

The authors of this paper succeeded in numerically modeling and simulating the corona discharge in the Wire-Cylinder-Plane geometry, a rather complex electrode configuration compared to the classical arrangements already treated in the literature. The validity and accuracy of the numerical model have been verified by a series of experimental results. The tests carried out made it possible to record the electric parameters of the corona discharge for different electrode arrangements in order to improve the performance of the charging process of the studied configuration. Overall, the experimental results show good agreement with numerical simulations.

It has been found that the presence of the non-ionizing cylinder above the ionizing wire has a significant influence on the development of the corona discharge causing, in particular, distortions of the electric field lines and the modification of the space charge density. The results showed that increasing the cylinder diameter, just like decreasing the distance between the wire and the cylinder, yields to the reduction of the corona discharge current and the current density recorded at the level of the ground plane. This is due to the shielding effect which is accentuated whenever the diameter of the cylinder is increased or when it is brought closer to the wire.

On the other hand, the use of the metal cylinder in the studied configuration allows a greater concentration of the field lines under the ionizing wire and makes it possible to obtain a controlled and localized deposit of charge.

Acknowledgement

The authors would like to express grateful acknowledgement to the DGRSDT (Direction Générale de la Recherche Scientifique et du Développement Technologique) for supporting the present work.

References

[1] M.P. Sarma, W. Janischewskyj, Analysis of Corona Losses on DC Transmission Lines: I—Unipolar Lines, IEEE Transactions on Power Apparatus and Systems. PAS-88 (1969) 718–731. https://doi.org/10.1109/TPAS.1969.292362.

[2] M. Abdel-Salam and Z. Al-Hamouz, A finite-element analysis of bipolar ionized field, IEEE Trans Ind Appl. 31 (1995) 477–483. https://doi.org/10.1109/28.382106

[3] A. Kasdi, Y. Zebboudj, H. Yala, Calculation and measurement of electric field under HVDC transmission lines, EPJ Applied Physics. 37 (2007) 323–329. https://doi.org/10.1051/epjap:2007026

[4] O.M. Bamigbola, M.M. Ali, M.O. Oke, Mathematical modeling of electric power flow and the minimization of power losses on transmission lines, Appl Math Comput. 241 (2014) 214–221. https://doi.org/10.1016/j.amc.2014.05.039

[5] A. Kasdi, Computation and measurement of corona current density and V–I characteristics in wires-to-plates electrostatic precipitator, J Electrostat. 81 (2016) 1–8. https://doi.org/10.1016/j.elstat.2016.02.005

[6] M. Gilliam, Polymer Surface Treatment and Coating Technologies, in: Handbook of Manufacturing Engineering and Technology, Springer London, 2013: pp. 1–23. https://doi.org/10.1007/978-1-4471-4976-7_20-3

[7] M.S. Bendilmi, T. Zeghloul, Z. Ziari, K. Medles, L. Dascalescu, Experimental characterization of electric potential uniformity at the surface of polymer plates corona charged by multiple-row needle-type electrodes, J Electrostat. 115 (2022). https://doi.org/10.1016/j.elstat.2021.103656

[8] S. Jodpimai, S. Boonduang, P. Limsuwan, Dielectric barrier discharge ozone generator using aluminum granules electrodes, J Electrostat. 74 (2015) 108–114. https://doi.org/10.1016/j.elstat.2014.12.003

[9] S. Tao, Y. Zhu, C. Chen, J. Liu, M. Chen, W. Shangguan, Removal of air pollutant by a spike-tubular electrostatic device: Multi-stage direct current corona discharge enhanced electrostatic precipitation and oxidation ability, Process Safety and Environmental Protection. 165 (2022) 347–356. https://doi.org/10.1016/j.psep.2022.06.069

[10] Q. Ye, J. Domnick, On the simulation of space charge in electrostatic powder coating with a corona spray gun, Powder Technol. 135–136 (2003) 250–260. https://doi.org/10.1016/j.powtec.2003.08.019

[11] L. M. Dumitran, P. V. Notingher, L. Dascalescu, Electrostatic Separation of Polymeric Granular Mixtures from Medium and Low Voltage Cables, the 9th International Symposium on Advanced Topics in Electrical Engineering, May 7-9, Bucharest, Romania, (2015**)** 507–510.

[12] H. Louati, A. Tilmatine, R. Ouiddir, A. Alibida, N. Zouzou, New separation technique of metal/polymer granular materials using an electrostatic sorting device, J Electrostat. 103 (2020). https://doi.org/10.1016/j.elstat.2019.103410

[13] M. Kachi, M. Nemamcha, B. Tabti, L. Dascalescu, Comparison between three measurement methods for characterizing the charge state of granular insulating materials, J Electrostat. 69 (2011) 394–400. https://doi.org/10.1016/j.elstat.2011.05.002

[14] M.C. Plopeanu, L. Dascalescu, B. Neagoe, A. Bendaoud, P. v. Notingher, Characterization of two electrode systems for corona-charging of non-woven filter media, J Electrostat. 71 (2013) 517–523. https://doi.org/10.1016/j.elstat.2012.12.002

[15] A. Reguig, A. Bendaoud, B. Neagoe, Y. Prawatya, L. Dascalescu, Electric potential distribution at the surface of insulating materials exposed to corona discharges from various electrode configurations, J Electrostat. 82 (2016) 55–62. https://doi.org/10.1016/j.elstat.2016.05.006

[16] O. Chibane, A. Rahmani, K. Smili, B. Bendahmane, L. Dascalescu, A. Kasdi, Experimental characterization of multi-wire corona electrode configurations, J Electrostat. 111 (2021). https://doi.org/10.1016/j.elstat.2021.103575

[17] M. Abdel-Salam, M. Nakano, A. Mizuno, Corona-induced pressures, potentials, fields and currents in electrostatic precipitator configurations, J Phys D Appl Phys. 40 (2007) 1919–1926. https://doi.org/10.1088/0022-3727/40/7/014

[18] J. Wang, T. Zhu, Y. xi Cai, J. fei Zhang, J. bo Wang, Review on the recent development of corona wind and its application in heat transfer enhancement, Int J Heat Mass Transf. 152 (2020). https://doi.org/10.1016/j.ijheatmasstransfer.2020.119545

[19] A. Messaoudene, L. Dascalescu, and B. Bendahmane, "Influence of high voltage waveform and frequency on the elimination of electric charges at the surface of polypropylene films", Rev. Roum. Sci. Techn.–Électrotechn. et Énerg. 67 (2022) 3–7.

[20] A. Reguig, L. Dascalescu, P. Dordizadeh, A. Bendaoud, Corona Discharge Generated by Dual-Type Electrode Fixed between Parallel Grounded Strips, IEEE Trans Ind Appl. 53 (2017) 1459–1465. https://doi.org/10.1109/TIA.2016.2637326

[21] M.B. Neagoe, Y.E. Prawatya, T. Zeghloul, L. Dascalescu, Electric-potential-measurement-based methodology for estimation of electric charge density at the surface of tribocharged insulating slabs, J Electrostat. 90 (2017) 123–130. https://doi.org/10.1016/j.elstat.2017.10.007

[22] A. Fatihou, L. Dascalescu, N. Zouzou, M.-B. Neagoe, A. Reguig, L.M. Dumitran, Measurement of Surface Potential of Non-uniformly Charged Insulating Materials Using a Non-contact Electrostatic Voltmeter, IEEE Transactions on Dielectrics and Electrical Insulation. 23 (2016) 2377–2384. https://doi.org/10.1109/TDEI.2016.7556516

[23] Y. Zebboudj, G. Hartmann, Current and electric field measurements in coaxial system during the positive DC corona in humid air, *EPJ Applied Physics*, 7 (1999) 167–176. https://doi.org/10.1051/epjap:1999211

[24] J. Lobry, A new numerical scheme for the simulation of corona fields, IEEE Trans Magn. 50 (2014) 541–544. https://doi.org/10.1109/TMAG.2013.2281999

[25] P. Dordizadeh, K. Adamiak, G.S. Peter Castle, Study of the impact of photoionization on negative and positive needle-plane corona discharge in atmospheric air, Plasma Sources Sci Technol. 25 (2016). https://doi.org/10.1088/0963-0252/25/6/065009

[26] N.A. Kaptzov, "Elektricheskie Invlentiia v Gazakh i Vakuumme", OGIZ Moscow (URSS) (1947) 587–630.

[27] F. W. Peek, "Dielectric phenomena in HV engineering", New York: McGraw-Hill, 1929.

[28] J.M. Townsend, Electricity in Gazes, Oxford University Press, 1915.

[29] M. Abdel-Salam and A. Eid, "Finite element simulation of corona in wire-duct precipitators," *Conference Record of the 2002 IEEE Industry Applications Conference. 37th IAS Annual Meeting (Cat. No.02CH37344)*, Pittsburgh, PA, USA, (2002) 1383–1389. https://doi.org/10.1109/IAS.2002.1042737

[30] Z. Al-Hamouz, A. El-Hamouz, N. Abuzaid, Simulation and experimental studies of corona power loss in a dust loaded wire-duct electrostatic precipitator, Advanced Powder Technology. 22 (2011) 706–714. https://doi.org/10.1016/j.apt.2010.10.005

[31] S. Arif, D.J. Branken, R.C. Everson, H.W.J.P. Neomagus, A. Arif, The influence of design parameters on the occurrence of shielding in multi-electrode ESPs and its effect on performance, J Electrostat. 93 (2018) 17–30. https://doi.org/10.1016/j.elstat.2018.03.001

[32] B. Chen, S. Li, Y. Guo, H. Li, W. Zhou, and B. Liu, Research on electrostatic shielding characteristics of electrostatic precipitator, Journal of the Air & Waste Management Association, Volume 72.4 (2022) 331–345. https://doi.org/10.1080/10962247.2021.2017374

[33] E. Warburg, Handbuch der physik, Chapter 14 (1927) 154–155.